Noise Temperatures and Gain Losses due to Leakage through Deep Space Network Antenna Perforated Panels at and above 32 Gigahertz

T. Y. Otoshi[1]

This article presents results of studying noise-temperature contributions due to leakage through the holes on perforated panels of the 34-m beam-waveguide (BWG) and 70-m antennas at 32 GHz and above. The noise-temperature contributions for the 34-m BWG antenna were 0.4 K at 32 GHz and increased to about 6 K at 45 GHz. For the 70-m antenna, the noise-temperature contribution was 0.8 K at 32 GHz and increased to about 16.4 K at 47 GHz. The highest frequencies at which the antennas were free of grating lobes were 45 GHz for the 34-m BWG antenna and 47 GHz for the 70-m antenna. It is conventional practice not to use antennas at and above any frequency at which grating lobes are generated.

I. Introduction

To reduce wind loading, the outer panels of DSN antennas are perforated. Figure 1 depicts the antenna with solid- and perforated-panel regions for an antenna pointed in the zenith direction. Leakage waves, which pass through holes in the perforated panels, are absorbed by the ground and contribute to the antenna noise temperature and gain loss. When the DSN antennas were designed (circa 1960), it was desired that the antennas operate satisfactorily at 2.295 GHz (S-band). Later it was desired that the antennas operate also at 8.450 GHz (X-band). To operate at X-band, it was necessary to reduce the size of the holes in the perforated panels. Wind tunnel tests by Katow[2] showed that a 3.175-mm (1/8-in.) hole diameter was as small as could be made for wind-loading relief purposes. Due to turbulence, panels with smaller diameters had the same wind loading as solid panels. It was found that leakage through 4.763-mm (3/16-in.)-diameter holes resulted in leakage losses that were about −30 dB at X-band [1], and leakage through 3.175-mm (1/8-in.)-diameter holes resulted in leakage losses close to −41 dB at X-band [2]. In recent years, requirements arose for DSN antennas to be operable with low noise at 32 GHz (Ka-band). The noise-temperature contribution due to leakage of panels on 34-m beam-waveguide (BWG) antennas was reported to be 0.67 K [2] at 32 GHz for the 34-m BWG antenna, as based on calculations through the use of an approximate method that was the best available in the 1990 era. No similar calculation was made for the 70-m antenna. For mechanical reasons not clear to this author, the thickness of the panels was reduced from 2.29 mm (0.090 in.) on 64-m antennas to 1.78 mm (0.070 in.) for the upgraded 70-m antennas and 34-m BWG antennas.

[1] Communications Ground Systems Section.

[2] S. Katow, personal communication, Jet Propulsion Laboratory, Pasadena, California, January 1963.

The research described in this publication was carried out by the Jet Propulsion Laboratory, California Institute of Technology, under a contract with the National Aeronautics and Space Administration.

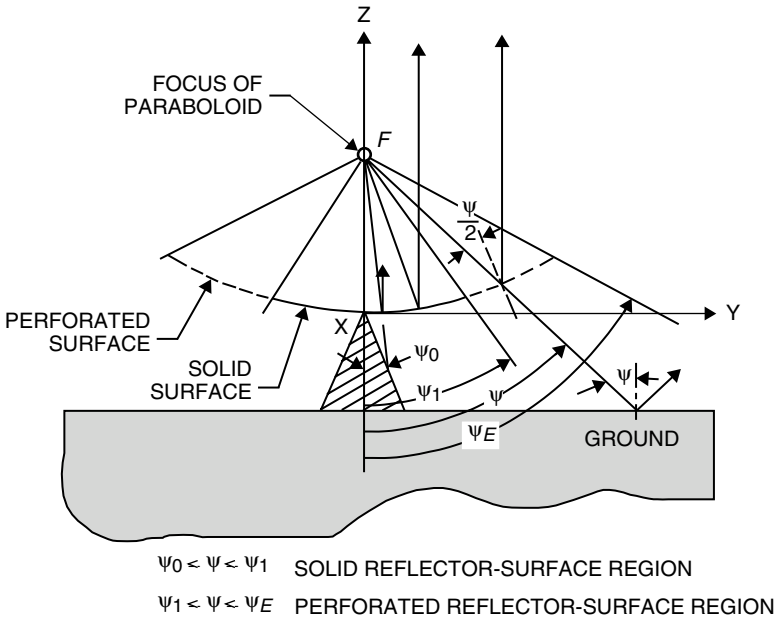

Fig. 1. Two-dimensional geometry of a zenith-oriented parabolic antenna with feed (or apparent feed) located at the focal point.

In recent years, many requests have been made of this author to provide calculations of noise-temperature contributions of particular DSN antennas at special radio science experiment frequencies above 32 GHz, such as 37 GHz, 41 GHz, and 50 GHz. The results for these higher frequencies have been provided in the form of informal notes by this author to the requestors, but this information was not documented in any formal report.

It is the purpose of this article to formally document the results for all frequencies at and above 32 GHz to as high a frequency as these perforated panels can be used before grating lobes cause excessive degradation of performance. Section II of this article discusses the numerical integration technique that was employed to make these calculations of noise-temperature contributions and gain losses due to leakage through these perforated panels. Section III discusses the geometries of the perforated panels on both 34-m BWG and 70-m antennas, and Section IV presents the calculated results and plots of the data.

II. Methodology

A. Old Calculation Method

In previous informal reports, it was assumed that the noise-temperature contribution due to leakage through perforated panels can be calculated by choosing a mid-subreflector pattern angle (the average of ψ_1 and ψ_E shown in Fig. 1) and then calculating the leakage or transmission loss at the corresponding incidence angle of a wave impinging upon the perforated panel. The leakage power ratio was then multiplied by an effective ground noise temperature. This result, however, applied to a case in which all radiated power illuminated only the perforated panels. The contribution of only the perforated-panel leakage for the real case was calculated by multiplying the previous result by the ratio of the projected area of the perforated panels to the projected total reflector surface area. The projected area is that area that results when projected onto the aperture plane. It is not known how accurate the results were when using this methodology, but based on plane wave considerations, it was believed to be sufficiently accurate when used for frequencies below 32 GHz. However, since the perforated plates no longer appear isotropic at higher frequencies and because the leakage through the plates becomes increasingly large, a more accurate method was needed for calculating noise temperature at higher frequencies above 32 GHz.

Theoretical formulas and the methodology used for computing antenna noise-temperature contributions and gain losses at the higher frequencies are presented in the following.

B. New Calculation Method

1. Noise Temperature Contribution. Reflector surface losses that increase antenna noise temperature are (1) ohmic losses of the metal and paint used as the reflective surface material and (2) leakage loss of RF energy passing through the perforated surface. Most of the energy that leaks through the surface is absorbed by the ground environment. To obtain estimates of the noise contributions from these two types of absorptive losses, approximate formulas have been derived. These are presented in the following section. Most of this material was extracted from an earlier article by Otoshi [3].

For a zenith-oriented parabolic antenna with circular symmetry, such as that shown in Fig. 1, the antenna noise temperature is

$$T_A = \frac{\int_0^{2\pi} \int_0^{\pi} T_b(\psi, \phi) P(\psi, \phi) \sin \psi d\psi d\phi}{\int_0^{2\pi} \int_0^{\pi} P(\psi, \phi) \sin \psi d\psi d\phi} \tag{1}$$

where

$T_b(\psi, \phi) =$ effective brightness temperature function as defined at the focal point F (Fig. 1), K

$P(\psi, \phi) =$ power per unit solid angle radiated by the feed or apparent feed at focal point F

$\psi =$ polar angle

$\phi =$ azimuthal angle

For purposes of this study, it is convenient to let Eq. (1) be expressed in terms of contributions from specific sources as

$$T_A = T'_A + (\Delta T_A)_{OL} + (\Delta T_A)_{LL} \tag{2}$$

where

$T'_A =$ total antenna temperature when the reflector surface has no ohmic and leakage losses, K

$(\Delta T_A)_{OL} =$ antenna noise-temperature contribution due to reflector surface ohmic losses, K

$(\Delta T_A)_{LL} =$ antenna noise-temperature contribution due to reflector surface leakage losses, K

It shall be assumed that the power per unit solid angle as radiated from the focal point is of the form ([4], Eq. 10, p. 263)

$$P(\psi, \phi) = \frac{1}{2\eta_0} \left[|A_1(\psi)|^2 \sin^2 \phi + |B_1(\psi)|^2 \cos^2 \phi \right] \tag{3}$$

where

$|A_1(\psi)| =$ E-plane amplitude pattern

$|B_1(\psi)| =$ H-plane amplitude pattern

$\eta_0 = 120\pi =$ free-space wave impedance, ohms

After substitutions of Eq. (3) and the appropriate brightness-temperature functions into Eq. (1) and integrations with respect to ϕ, it can be shown that

$$(\Delta T_A)_{OL} \simeq \frac{\left(\frac{4R_s}{\eta_0}\right) T_P \int_{\psi_0}^{\psi_E} [1-\alpha(\psi)] \left[p_1(\psi) \sec\frac{\psi}{2} + p_2(\psi)\cos\frac{\psi}{2}\right] \sin\psi d\psi}{\int_0^{\pi} [p_1(\psi)+p_2(\psi)] \sin\psi d\psi} \tag{4}$$

and the equation for noise temperature due to leakage through perforated panels is

$$(\Delta T_A)_{LL} = \frac{\int_{\psi_1}^{\psi_E} T_G(\psi) \left[t_{//}(\psi)p_1(\psi) + t_{\perp}(\psi)p_2(\psi)\right] \sin\psi d\psi}{\int_0^{\pi} [p_1(\psi)+p_2(\psi)] \sin\psi d\psi} \tag{5}$$

where $(\Delta T_A)_{OL}$ and $(\Delta T_A)_{LL}$ were defined in Eq. (2) and

$p_1(\psi) = \left|\frac{A_1(\psi)}{A_1(0)}\right|^2$

$p_2(\psi) = \left|\frac{B_1(\psi)}{A_1(0)}\right|^2$

$T_P =$ physical temperature of the reflector surface, K

$R_S =$ surface resistivity of the reflector surface material, ohms/square (a function of frequency and electrical conductivity [5])

$\alpha(\psi) =$ porosity of the unit cell of the reflector surface, equal to zero for $\psi_0 < \psi \leq \psi_1$ over the solid-panel region, and equal to $\pi d^2/(4s^2 \sin 60 \text{ deg})$ for $\psi_1 < \psi \leq \psi_E$ over the perforated-panel region, where d and s are, respectively, the hole diameter and hole-to-hole spacing of the perforated plate (see Fig. 2)

$T_G(\psi) =$ effective ground noise-temperature function ([6], Eq. 21, p. 210)

$t_{//}(\psi) =$ leakage power-loss ratio for an incident wave with the E-field polarized parallel to the plane of incidence; this loss in positive dB will be referred to as the transmission loss for parallel polarization

$t_{\perp}(\psi) =$ leakage power-loss ratio for an incident wave with the E-field polarized perpendicular to the plane of incidence; this loss in positive dB will be referred to as the transmission loss for perpendicular polarization

$\psi_0, \psi_1, \psi_E =$ polar angles defining boundaries of the solid and perforated reflector surface regions, respectively (Fig. 1)

Referring to the geometry of Fig. 2, for a parabolic antenna whose surface is perforated periodically with circular holes, $t_{//}(\psi)$ and $t_{\perp}(\psi)$ can be calculated through the use of a computer program provided by C. C. Chen employing the equations given in [7]. If only approximate values are needed below 32 GHz, then the approximate Otoshi formulas given in [1,3] can be used.

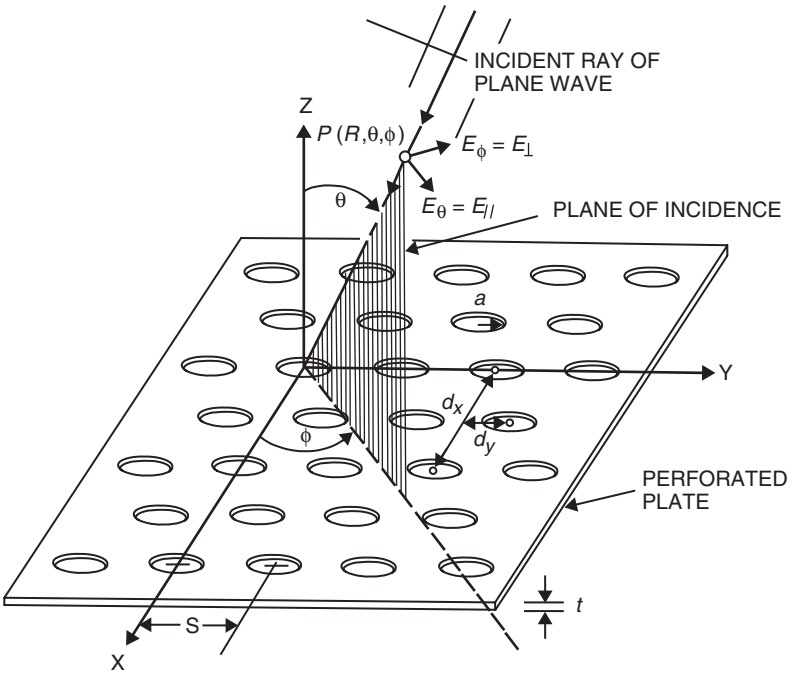

Fig. 2. Perforated plate geometry with an obliquely incident plane wave polarized with the E-field perpendicular and parallel to the plane of incidence.

For this article, it will be assumed that there are no losses due to finite metal conductivity and paint. Therefore, in Eq. (4), it will be assumed that $R_S = 0$ and $(\Delta T_A)_{OL} = 0$. If one wishes to compute ohmic losses of a DSN antenna, one can use the value of R_S for a painted aluminum surface given in [5] and use that value in Eq. (4).

For circular polarization, let $p_1(\psi) = p_2(\psi) = p(\psi)$ in Eq. (5). Then noise temperature due to leakage through perforated panels becomes

$$(\Delta T_A)_{LL} = \frac{\int_{\psi_1}^{\psi_E} T_G(\psi) p(\psi) t_E(\psi) \sin\psi d\psi}{\int_0^{\pi} p(\psi) \sin\psi d\psi} \tag{6}$$

where $t_E(\psi)$ is the effective power transmission coefficient expressed as

$$t_E(\psi) = \frac{t_{//}(\psi) + t_\perp(\psi)}{2} \tag{7}$$

For best accuracy, $p(\psi)$ should be determined from subreflector patterns at every frequency of interest. For simplicity, it will be assumed that $p(\psi)$ does not change with frequency and the following conditions exist:

$$p(\psi) = 0 \text{ for } 0 \le \psi < \psi_0$$

$$p(\psi) = 1 \text{ for } \psi_0 \le \psi \le \psi_E$$

$$p(\psi) = 0 \text{ for } \psi_E < \psi \le \pi$$

where ψ_0 is the subreflector angle at which the solid-panel section begins. Normally for a focal-point-fed parabola, ψ_0 would be zero, but for DSN Cassegrain antennas, ψ_0 is an angle that is from 2 to 6 deg. For example, for the 34-m BWG antenna, the solid-panel section actually begins at the outer edge of the BWG hole opening on the main-reflector surface. For the 70-m antenna, the solid-panel section begins at the outer circumference of the cylindrically shaped Mod III section.

Application of the above assumptions to Eq. (5) leads to the denominator of Eq. (5) becoming

$$D = \int_0^{\pi} p(\psi) \sin\psi d\psi = \int_{\psi_0}^{\psi_E} \sin\psi d\psi$$

$$= \cos\psi_0 - \cos\psi_E \tag{8}$$

The numerator of Eq. (5) becomes

$$N = \int_{\psi_1}^{\psi_E} T_G(\psi) t_E(\psi) \sin\psi d\psi \tag{9}$$

It was assumed that $t_E(\psi)$ is independent of ϕ. While this was nearly true for DSN antenna perforated panels at frequencies below 32 GHz, the assumption becomes increasingly invalid as frequencies go above 40 GHz. The method used to partially overcome the problem was to compute $t_E(\psi, \phi)$ over the range of $0 \leq \phi < 2\pi$ and then to compute an average $t_E(\psi, \phi)$ and assume that the average value could be used for $t_E(\psi)$ in Eq. (9). The brightness-temperature function $T_G(\psi)$ was assumed to be independent of ϕ because the antenna is assumed to be located above a flat desert ground environment [6]. Furthermore, it is the practice to assume that $T_G(\psi)$ can be replaced by an effective ground brightness temperature, T_{GE}, that is a constant. For DSN antennas and a flat desert ground, a value of 268 K is assigned for zenith-pointing antennas [2]. Equation (9) then becomes

$$N = T_{GE} \int_{\psi_1}^{\psi_E} t_E(\psi) \sin\psi d\psi \tag{10}$$

The parameter $t_E(\psi)$ varies slowly over the reflector surface so that numerical integration methods can be employed over rather wide intervals. For this article, the integration was performed over four regions of integrations of equal widths computed from

$$\Delta\psi = \left(\frac{\psi_E - \psi_1}{5}\right) \tag{11}$$

$$\psi_{i+1} - \psi_i = \Delta\psi \quad \text{for } i = 1, 4 \tag{12}$$

Now Eq. (6) can be written as

$$(\Delta T_A)_{LL} = \sum_{i=1}^{4} T_i \tag{13}$$

where

$$T_i = \frac{T_{GE}\overline{t_{Ei}}}{D}\int_{\psi_i}^{\psi_{i+1}} \sin\psi_i d\psi$$

$$= \frac{T_{GE}\overline{t_{Ei}}}{D}\left(\cos\psi_i - \cos\psi_{i+1}\right) \quad \text{for } i = 1, 4 \tag{14}$$

Note that when $i = 4$, $\psi_5 = \psi_E$; and $\overline{t_{Ei}}$ is the average $t_E(\psi)$ over the interval ψ_i to ψ_{i+1} computed from

$$\overline{t_{Ei}} = \frac{t_E(\psi_i) + t_E(\psi_{i+1})}{2} \tag{15}$$

and the expression for $t_E(\psi)$ was given in Eq. (7).

2. Gain Loss. Consider the reflections off the paraboloidal surface as shown in Fig. 1. Using the same assumptions used to derive the noise-temperature equation, the total effective-power reflection coefficient becomes

$$|\Gamma_E|^2 = \frac{1}{D}\int_{\psi_0}^{\psi_E} |\Gamma(\psi)|^2 \, p(\psi) \sin\psi d\psi \tag{16}$$

where the expression for D was given in Eq. (8). It is assumed that the power reflection coefficient $|\Gamma(\psi)|^2$ is a function of ψ only and not also of ϕ. In the absence of ohmic losses,

$$|\Gamma(\psi)|^2 = 1 - t_E(\psi) \tag{17}$$

where $t_E(\psi)$ was defined in Eq. (7). If the integration is performed over the solid- and perforated-panel sections numerically, Eq. (16) can be written as

$$|\Gamma_E|^2 = I_0 + \sum_{i=1}^{4} I_i \tag{18}$$

where I_0 is the integrated value for the solid-panel section, expressed as

$$I_0 = \frac{1}{D}\int_{\psi_0}^{\psi_1} |\Gamma(\psi)|^2 \, p(\psi) \sin\psi d\psi \tag{19}$$

and, assuming that $p(\psi) = 1$ and $|\Gamma(\psi)|^2 = 1$ over the interval $\psi = \psi_0$ to ψ_1, the expression given in Eq. (19) reduces to

$$I_0 = \frac{\cos\psi_0 - \cos\psi_1}{D} \tag{20}$$

for the perforated-panel regions, again subdividing it into the same four regions as was done for noise temperature. Then, for $i = 1$ to 4,

$$I_i = \frac{1}{D}\int_{\psi_i}^{\psi_{i+1}} |\Gamma(\psi)|^2 \, p(\psi) \sin\psi$$

$$= \frac{1}{D}\left|\overline{\Gamma(\psi_i)}\right|^2 (\cos\psi_i - \cos\psi_{i+1}) \tag{21}$$

where

$$\left|\overline{\Gamma\,(\psi_i)}\right|^2 = 1 - \overline{t_{Ei}} \tag{22}$$

where $\overline{t_{Ei}}$ was given in Eq. (15).

Then, substitutions into Eq. (16) give

$$|\Gamma_E|^2 = \frac{1}{D}(\cos\psi_0 - \cos\psi_1) + \frac{1}{D}\sum_{i=1}^{4}\left(1 - \overline{t_{Ei}}\right)(\cos\psi_i - \cos\psi_{i+1}) \tag{23}$$

and gain loss in decibels is

$$(G_L)_{dB} = 10\log|\Gamma_E|^2 \tag{24}$$

III. Perforated-Plate and -Panel Geometries

Figure 2 shows the perforated-plate geometry for an incident wave where the E-field is polarized perpendicular and parallel to the incidence plane. The angle of incidence upon the plate is the angle θ and is equal to 1/2 the subreflector angle ψ, shown in Fig. 1. The angle ϕ is the spherical coordinate system azimuthal angle that defines the orientation of the plane of incidence about the z-axis. The rows of holes are staggered to form an equilateral-triangle pattern arrangement. For circular polarization, the angle ϕ varies from 0 to 360 deg, but the properties for this equilateral-triangle hole-pattern arrangement repeat every 60 deg. For this study, calculations were made with the ϕ angle varying from 0 to 90 deg in 10-deg increments, and then the results were averaged. The needed parameters for calculating leakage are the plate parameters d, s, and t, shown in Fig. 2, which, respectively, are hole diameter, hole-to-hole spacing, and plate thickness. For both the 34-m and 70-m antennas, d, s, and t are 3.2 mm (1/8 in.), 4.8 mm (3/16 in.), and 1.8 mm (0.070 in.), respectively.

The main reflectors on 34-m beam-waveguide (BWG) antennas are paneled with curved, solid-sheet panels starting from the BWG opening radius of 1.2 m and going to 13 m radially out from the main-reflector z-axis (Fig. 1). Then the perforated panels go out from the 13-m radius to an outer reflector edge radius of 17 m. This results in the perforated area being 41.74 percent of the total reflector surface area as projected on the aperture plane. The subreflector angles ψ at the beginning of the perforated section and at the outer edge of the panel sections were calculated to be 61.2 and 75.6 deg, respectively (see Fig. 1).

For 70-m antennas, the solid-sheet panels go from a Mod III section outer radius of 3.2 m out to 18.788 m. Then perforated panels begin at the 18.788-m (739.688-in.) radius and go out to the outer reflector edge of 35.0107 m (1378.375 in.). The ratio of the perforated-panel area to the total actual

reflector area is calculated to be 71.8 percent. The subreflector angles at the beginning of the perforated section and at the outer edge of the panel sections were calculated to be 38.2 and 65.8 deg, respectively, where the subreflector angle, ψ, can be seen depicted in Fig. 1.

The subreflector angle from the focal point to a point on an assumed parabolic surface can be calculated from

$$\psi = 2\tan^{-1}\left(\frac{\rho}{2F}\right) \tag{25}$$

and the incidence angle at the reflection point is

$$\theta = \frac{\psi}{2} \tag{26}$$

where

$\rho =$ radius from the paraboloid central z-axis to a point on the parabolic surface

$F =$ paraboloid focal length

If ρ is not known but ψ is known, then ρ can be calculated from

$$\rho = 2F\tan\left(\frac{\psi}{2}\right) \tag{27}$$

The main parabola focal length, F, is equal to 11.68 m (460 in.) for the 34-m BWG antenna and 28.89 m (1137.3 in.) for the 70-m antenna. Other pertinent data needed to perform the integrations of the formulas given in Section II are as follows.

A. 34-m BWG Antenna

Solid-Panel Region:

(1) ψ is between 5.97 deg and 58.18 deg

(2) ρ is between 1.22 m (48 in.) and 13 m (511.8 in.)

Region 1:

(1) ψ is between 58.18 deg and 61.654 deg

(2) Incidence angle θ is between 29.08 deg and 30.83 deg

(3) ρ is between 13 m (511.8 in.) and 13.944 m (548.97 in.)

Region 2:

(1) ψ is between 61.654 deg and 65.13 deg

(2) Incidence angle θ is between 30.83 deg and 32.57 deg

(3) ρ is between 13.944 m (548.97 in.) and 14.923 m (587.5 in.)

Region 3:

(1) ψ is between 65.13 deg and 68.6 deg

(2) Incidence angle θ is between 32.57 deg and 34.3 deg

(3) ρ is between 14.92 m (587.5 in.) and 15.94 m (627.56 in.)

Region 4:

(1) ψ is between 68.6 deg and 72.1 deg

(2) Incidence angle θ is between 34.3 deg and 36.04 deg

(3) ρ is between 15.94 m (627.56 in.) and 17 m (669.3 in.)

B. 70-m Antenna

Solid-Panel Region:

(1) ψ is between 2.42 deg and 36.04 deg

(2) ρ is between 1.22 m (48 in.) and 18.79 m (739.7 in.)

Region 1:

(1) ψ is between 36.04 deg and 42.64 deg

(2) Incidence angle θ is between 18.02 deg and 21.32 deg

(3) ρ is between 18.79 m (739.7 in.) and 22.54 m (887.5 in.)

Region 2:

(1) ψ is between 42.64 deg and 49.24 deg

(2) Incidence angle θ is between 21.32 deg and 24.62 deg

(3) ρ is between 22.54 m (887.5 in.) and 26.47 m (1042.1 in.)

Region 3:

(1) ψ is between 49.24 deg and 55.84 deg

(2) Incidence angle θ is between 24.62 deg and 27.92 deg

(3) ρ is between 26.47 m (1042.1 in.) and 30.61 m (1205.1 in.)

Region 4:

(1) ψ is between 55.84 deg and 62.44 deg

(2) Incidence angle θ is between 27.92 deg and 31.22 deg

(3) ρ is between 30.61 m (1205.1 in.) and 35.01 m (1378.4 in.)

IV. Results

The transmission loss in decibels for this geometry as a function of frequency at and above 32 GHz is shown in Figs. 3 and 4, respectively, for the 34-m BWG and 70-m antennas. They were calculated for subreflector angles midway between ψ_1 and ψ_E, and the corresponding incidence angle thetas were $\psi/2$. These losses were calculated through the use of a FORTRAN computer program furnished to JPL by C. C. Chen [7]. In a previous article [1], the same program was used to compute the transmission losses from 1 GHz to 45 GHz for perforated panels on the 64-m DSN antenna. At the time the article [1] was written, the 64-m antenna had panels with a larger hole diameter of 4.763 mm (0.1875 in.), larger hole-to-hole spacing of 6.350 mm (0.250 in.), and larger thickness of 2.286 mm (0.090 in.). The larger hole diameter and spacing for the 64-m antenna caused the transmission loss to become 0 dB at about 43 GHz for a 0-deg incidence angle, and the first grating lobe appeared at 37 GHz for a 30-deg incidence angle. The perforated panels on the current 34-m BWG and 70-m antennas enable operation at a higher frequency with acceptable noise contribution and gain losses.

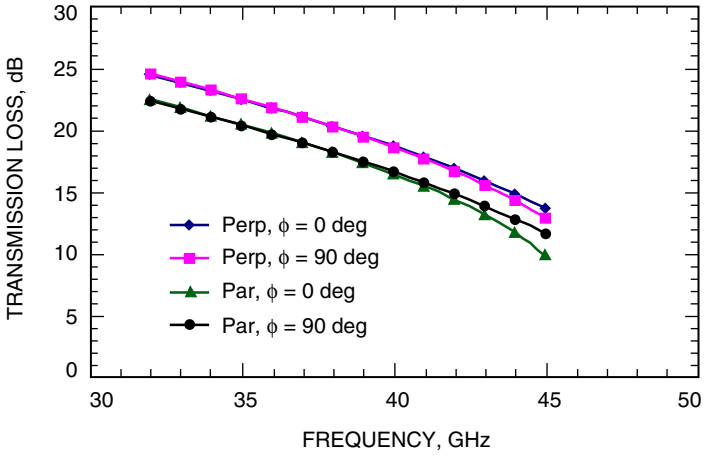

Fig. 3. The 34-m BWG antenna perforated-panel transmission loss at and above 32 GHz for psi = 65.13 deg ("Perp" and "Par" are perpendicular and parallel polarizations, respectively). Invalid beyond 45 GHz due to grating lobes.

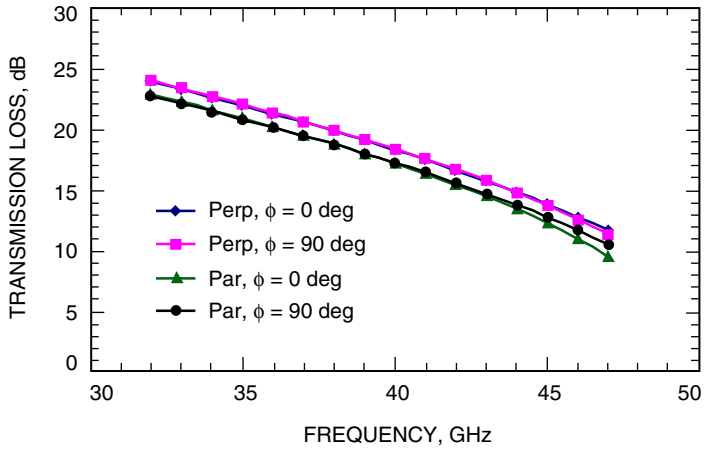

Fig. 4. The 70-m antenna perforated-panel transmission loss at and above 32 GHz for psi = 49.2 deg ("Perp" and "Par" are perpendicular and parallel polarizations, respectively). Grating lobes occur at 48 and 49 GHz.

The plots shown in Figs. 3 and 4 for the current DSN antennas are for transmission losses for the E-field perpendicular and parallel to the plane of incidence for azimuth angles $\phi = 0$ and 90 deg. For circular polarization, the transmission losses in dB are converted to power ratios, and the average is taken of the power ratios of perpendicular and parallel polarizations. Figures 3 and 4 show that, for the 34-m BWG and 70-m antennas, the transmission losses are about -10 dB at their highest permissible frequencies of operation. Grating lobes appear at frequencies above 45 GHz for the 34-m BWG antenna and above 47 GHz for the 70-m antenna and do not obey Snell's Laws of Reflection and Transmission. Therefore, no calculations of noise temperatures are attempted when grating lobes appear.

The results of calculations of noise-temperature contributions for the 34-m antenna are shown in Table 1 and plotted in Fig. 5 for 32-GHz frequencies and above. Figure 5 shows the contribution from each region and also the total from all four regions of integration. Calculations could not be made above 45 GHz because grating lobes occur in the outer perforated-panel regions. Table 2 and Fig. 6 show similar data for the 70-m antenna. The noise temperature is a function of ϕ as well as θ. To partially overcome this problem, noise temperature was computed at $\phi = 0$ deg and then again for a new ϕ increased by 10 deg until $\phi = 90$ deg was reached. Then the average noise-temperature contribution and the standard deviation (SD) from the average were computed and plotted. For the 34-m BWG antenna, the perforated-

Table 1. The 34-m BWG antenna perforated-panel, circular-polarization noise-temperature contributions averaged over phi 0 to 90 deg (effective ground brightness temperature = 268 K).

Frequency, GHz	Region 1 Avg NT, K	Region 2 Avg NT, K	Region 3 Avg NT, K	Region 4 Avg NT, K	Total (regions 1–4)	
					Avg NT, K	Std dev, K
32	0.095	0.098	0.101	0.104	0.398	0.002
33	0.110	0.114	0.117	0.120	0.462	0.002
34	0.128	0.133	0.137	0.141	0.538	0.003
35	0.150	0.155	0.160	0.165	0.630	0.004
36	0.176	0.182	0.188	0.194	0.741	0.005
37	0.208	0.216	0.224	0.232	0.880	0.009
38	0.247	0.257	0.267	0.277	1.047	0.009
39	0.295	0.309	0.322	0.335	1.261	0.013
40	0.357	0.375	0.393	0.411	1.535	0.020
41	0.436	0.460	0.486	0.513	1.895	0.033
42	0.540	0.575	0.612	0.655	2.382	0.058
43	0.680	0.733	0.792	0.865	3.071	0.114
44	0.878	0.962	1.066	1.212	4.119	0.262
45	1.169	1.321	1.545	1.987	6.022	0.841
46	1.639	1.985	2.816	Invalid	Invalid	Invalid
47	2.554	4.049	Invalid	Invalid	Invalid	Invalid
48	5.255	Invalid	Invalid	Invalid	Invalid	Invalid
49	Invalid	Invalid	Invalid	Invalid	Invalid	Invalid

Notes:

1. "NT" is the noise temperature; "Avg" and "Std dev" are the average and the standard deviation of the average based on values at 10 phi angles going from 0 to 90 deg in 10-deg increments.
2. If it is necessary to use the total perforated-panel areas for maximum gain, do not use the 34-m antenna above 45 GHz. At 45 GHz, the worst-case NT contribution will be 6.02 ± 0.84 K.

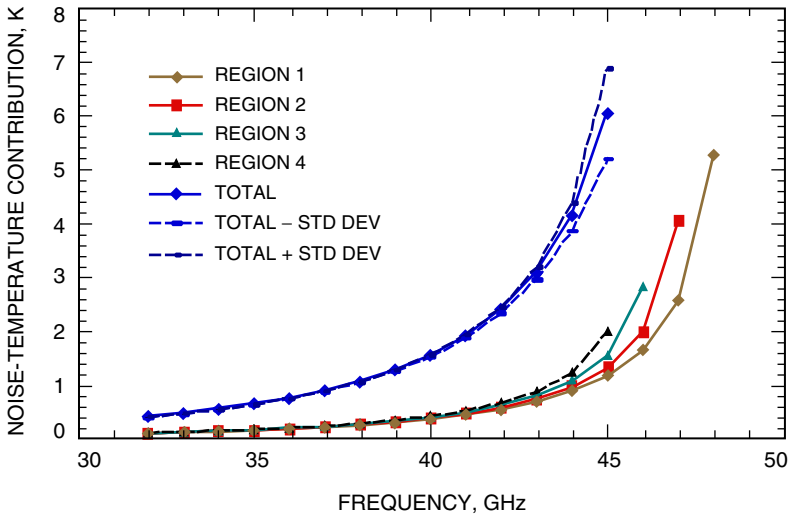

Fig. 5. The 34-m BWG antenna perforated-panel noise-temperature contributions at and above 32 GHz. The total beyond 45 GHz is invalid due to grating lobes.

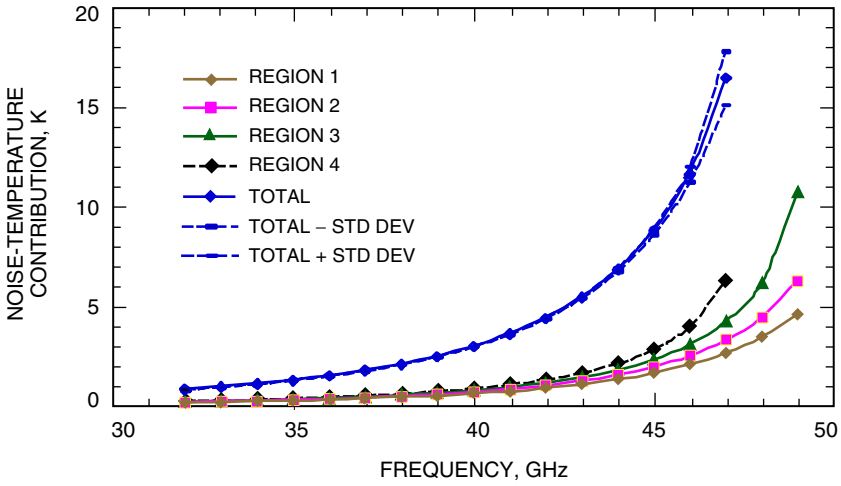

Fig. 6. The 70-m antenna perforated-panel noise-temperature contributions. Invalid above 47 GHz due to grating lobes in region 4.

panel noise-temperature contribution is about 0.4 K at 32 GHz and increases to 6.0 K at 45 GHz. For the 70-m antenna, the perforated-panel noise-temperature contribution is 0.82 K at 32 GHz and increases to 16.4 K at 47 GHz.

The antenna can be used at and above the grating-lobe-occurrence frequencies if the feed can be designed to illuminate inner perforated-panel regions only, as shown in Table 3. If this can be done, then calculations show that the perforated-panel noise-temperature contributions are about 8.2 K at 46 GHz for the 34-m BWG antenna and 26.5 K at 49 GHz for the 70-m antenna, as shown in Table 3. However, by under-illuminating the main-reflector surface, total antenna gain will become significantly lowered just due to the fact that the antenna aperture area is significantly decreased.

It is of interest to compare the results of the new method against the old method of calculating noise-temperature contribution for a parabolic antenna (see Section II). When using the same average power

Table 2. The 70-m antenna perforated-panel, circular-polarization noise-temperature contributions averaged over phi 0 to 90 deg (effective ground brightness temperature = 268 K).

Frequency, GHz	Region 1 Avg NT, K	Region 2 Avg NT, K	Region 3 Avg NT, K	Region 4 Avg NT, K	Total (regions 1–4)	
					Avg NT, K	Std dev, K
32	0.174	0.196	0.215	0.231	0.816	0.002
33	0.201	0.226	0.249	0.268	0.944	0.003
34	0.233	0.262	0.289	0.312	1.096	0.003
35	0.270	0.305	0.336	0.365	1.277	0.004
36	0.315	0.357	0.394	0.428	1.494	0.005
37	0.369	0.418	0.463	0.505	1.756	0.006
38	0.434	0.493	0.549	0.600	2.076	0.008
39	0.513	0.585	0.653	0.718	2.469	0.010
40	0.610	0.698	0.784	0.867	2.959	0.013
41	0.731	0.840	0.950	1.059	3.579	0.019
42	0.881	1.020	1.162	1.311	4.374	0.029
43	1.073	1.251	1.440	1.649	5.414	0.047
44	1.318	1.554	1.813	2.123	6.808	0.083
45	1.639	1.957	2.328	2.820	8.744	0.167
46	2.065	2.511	3.075	3.955	11.606	0.388
47	2.643	3.292	4.219	6.257	16.412	1.339
48	3.450	4.448	6.191	Invalid	Invalid	Invalid
49	4.611	6.268	10.695	Invalid	Invalid	Invalid

Notes:

1. "NT" is the noise temperature; "Avg" and "Std dev" are the average and the standard deviation of the average based on values at 10 phi angles going from 0 to 90 deg in 10-deg increments.
2. If it is necessary to use the total perforated-panel areas for maximum gain, do not use the 34-m antenna above 47 GHz. At 47 GHz, the worst-case NT contribution will be 16.4 ± 1.34 K.

Table 3. Summary of results for the 34-m BWG antenna and 70-m antenna illuminating the solid panels and only the perforated-panel regions having no grating lobes.

Frequency, GHz	Illuminate only regions	Total NT, K	Std dev, K
34-m BWG antenna			
46	1, 2, and 3	7.02	1.51
47	1 and 2	7.90	2.57
48	1	6.95	2.66
70-m antenna			
48	1, 2, and 3	16.40	0.96
49	1, 2, and 3	26.51	3.34

transmission coefficient and effective ground brightness temperature for both methods, for the 34-m BWG antenna the new method gave 0.40 ± 0.002 K versus 0.52 ± 0.003 K for the old method at 32 GHz. The tolerances are the standard deviation due to ϕ variations. At 45 GHz, the new method gave 6.02 ± 0.84 K versus 7.34 ± 0.63 K using the old method. For the 70-m antenna, the new method gave 0.82 ± 0.002 K versus 0.90 ± 0.002 K using the old method at 32 GHz, and at 45 GHz the new method gave 8.74 ± 0.17 K versus 9.30 ± 0.09 K using the old method. Better agreement was obtained between values from the new and the old methods for the 70-m antenna. The closeness of the results of the new method versus the old method seems to be related to the porosities of the two antennas, which is 41.7 percent for the 34-m BWG antenna and 71.8 percent for the 70-m antenna. Porosity here is defined as the ratio of the total perforated panel area to the total reflector surface area of the antenna, where the areas are the areas as measured when projected on the aperture plane. At X-band or lower frequencies, it is reasonable to expect that less difference would be observed in values when calculating noise temperatures using the new method versus the old method.

Gain losses due to leakage through the perforated panels were calculated through use of formulas given in Section II and plotted in Figs. 7 and 8. Figure 7 shows the gain loss for the 34-m BWG antenna to be small (about -0.005 dB) at 32 GHz, but it increases to about -0.1 dB at 45 GHz. Figure 8 shows that, for the 70-m antenna, the gain loss is also small (about -0.01 dB) at 32 GHz, but it increases to about -0.28 dB at 47 GHz.

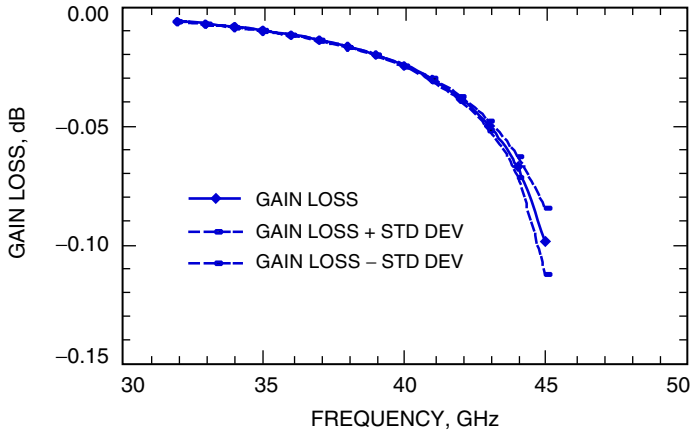

Fig. 7. The 34-m BWG antenna gain loss due to leakage through perforated panels at and above 32 GHz. Grating lobes exist beyond 45 GHz.

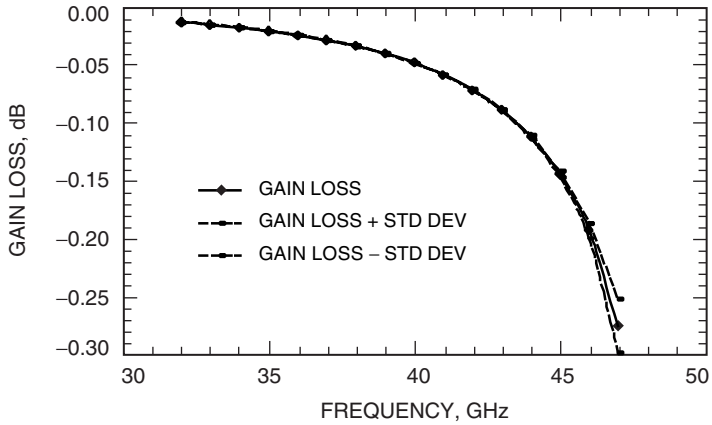

Fig. 8. The 70-m antenna gain loss due to leakage through perforated panels at and above 32 GHz. Grating lobes exist beyond 47 GHz.

V. Concluding Remarks

The noise temperature contributions and gain losses due to leakage through perforated panels on both the 34-m BWG antenna and 70-m antenna have been calculated and presented. For the 34-m antenna, calculations above 45 GHz could not be made due to grating lobes that occur. For the 70-m antenna, grating lobes occur above 47 GHz. The results are worst case because it was assumed that $p(\psi) = 1$ such that the subreflector pattern uniformly illuminates the main reflector for all angles of ψ. If the actual subreflector pattern is known, improved accuracy can be obtained if an average $p(\psi)$ is calculated for each of the regions 1 through 4 shown in Table 1 or Table 2. Then multiply this average $p(\psi)$ by the calculated noise-temperature values of the applicable region and frequency and compute the total contribution as shown in Table 1 or Table 2. Subreflector patterns can be quite different depending upon the frequency, feed, and subreflector design. A subreflector pattern at 2.1 GHz for a 64-m antenna was shown by Bathker (see Fig. 2 of [8]) to have a spike at $\psi = 0$ deg, followed by noticeable ripples. As ψ approached the edge of the main reflector, the pattern level began to drop rapidly. Subreflector patterns at 8.45 GHz for a shaped 64-m antenna were shown by Potter (see Figs. 4 through 6 of [9]) to be closer to the ideal case. Patterns at 8.45 GHz for a 26-m antenna subreflector with a vertex plate were shown by Williams and Reilly (see Fig. 5a of [11]) to have a deep null in the region of $\psi = 0$ deg.

It should be stated that these calculations of noise temperature contributions were made for the antennas pointing at zenith. An analysis by Otoshi [2] showed that simplification could be made by assuming that the effective ground brightness temperatures were 268, 214, and 166 K for the antenna pointed at 90-, 30-, and 10-deg elevation angles. These were based on assuming the leakage through the reflector with perforations was mostly absorbed by desert ground and the portions not absorbed were reflected and absorbed by the sky. To compute noise temperatures at a 30-deg elevation angle, it is necessary only to multiply all of the results presented in this article by the ratio 214/268. Similarly, the noise temperatures at 10-deg elevation angles can be obtained by multiplying the results by the ratio 166/268. It is assumed that the strut supports do not scatter or contribute to noise temperature. The reason why the noise-temperature contributions become lower with elevation angle is that less of the leakage sees the ground when the antenna is pointed at low elevation angles. In the ideal case, for an antenna pointed at the horizon, half of the leakage goes up to the sky region.

These results should be quite useful for radio scientists who are wondering if the DSN antennas can be used at frequencies higher than 32 GHz for radio science experiments.

References

[1] T. Y. Otoshi, "RF Properties of the 64-m-Diameter Antenna Mesh Material as a Function of Frequency," *The Deep Space Network Progress Report for September and October 1972,* Technical Report 32-1526, vol. XII, Jet Propulsion Laboratory, Pasadena, California, pp. 26–31, December 15, 1972. http://tmo.jpl.nasa.gov/tmo/progress_report2/XII/XIIG.PDF

[2] D. A. Bathker, W. Veruttipong, T. Y. Otoshi, and P. W. Cramer, Jr., "Beam Waveguide Antenna Performance Predictions with Comparisons to Experimental Results," *Microwave Theory and Techniques,* Special Issue (Microwaves in Space), vol. MTT-40, no. 6, pp. 1274–1285, June 1992.

[3] T. Y. Otoshi, "Antenna Noise Temperature Contributions Due to Ohmic and Leakage Losses of the DSS 14 64-m Antenna Reflector Surface," *The Deep Space Network Progress Report for July and August 1971,* Technical Report 32-1526, vol. V, Jet Propulsion Laboratory, Pasadena, California, pp. 115–119, October 15, 1971.
http://tmo.jpl.nasa.gov/tmo/progress_report2/V/VR.PDF

[4] T. Otoshi and C. T. Stelzried, "Antenna Temperature Analysis," *Space Programs Summary 37-36,* vol. IV, Jet Propulsion Laboratory, Pasadena, California, pp. 262–267, December 31, 1965.

[5] T. Y. Otoshi and M. M. Franco, "The Electrical Conductivities of Steel and Other Candidate Material for Shrouds in a Beam-Waveguide Antenna System," *IEEE Trans. on Instrumentation and Measurement,* vol. IM-45, no. 1, pp. 77–83, February 1996. (Correction in *IEEE Trans. on Instrumentation and Measurement,* vol. IM-45, no. 4, p. 839, August 1996.)

[6] T. Otoshi, "Antenna Temperature Analysis," *Space Programs Summary 37-37,* vol. IV, Jet Propulsion Laboratory, Pasadena, California, pp. 207–210, February 28, 1966.

[7] C. C. Chen, "Transmission of Electromagnetic Waves by Conducting Screen Perforated Periodically with Circular Holes," *IEEE Trans. on Microwave Theory Tech.,* vol. MTT-19, no. 5, pp. 475–481, May 1971.

[8] D. A. Bathker, *Predicted and Measured Power Density Description of a Large Ground Microwave System,* JPL Technical Memorandum 33-433, Jet Propulsion Laboratory, Pasadena, California, April 15, 1971.

[9] P. D. Potter, "Shaped Antenna Designs and Performance for 64-m Class DSN Antennas," *The Deep Space Network Progress Report 42-20, January and February 1974,* Jet Propulsion Laboratory, Pasadena, California, pp. 92–111, April 15, 1974.
http://tmo.jpl.nasa.gov/tmo/progress_report2/42-20/20P.PDF

[10] W. Williams and H. Reilly, "A Prototype DSN X/S-Band Feed: DSS 13 Application Status (Fourth Report)," *The Telecommunications and Data Acquisition Progress Report 42-60,* Jet Propulsion Laboratory, Pasadena, California, pp. 77–88, December 15, 1980.
http://tmo.jpl.nasa.gov/tmo/progress_report/42-60/60I.PDF